

EDARD-TR-91-04

(2)

Studies of Plasma Irregularities and Convection in the Polar Ionosphere using
HILAT, SABRE and EISCAT

AD-A232 983

T.B. Jones
M. Lester

Ionospheric Physics Group
Department of Physics,
University of Leicester,
Leicester, LE1 7RH,
United Kingdom.

DTIC
ELECTE
MAR 11 1991
S D

FINAL REPORT

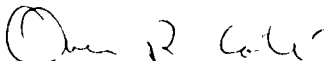
EXEMPTION STATEMENT A
Approved for public release
Distribution Unlimited

91 3 05 094

EOARD-TR-91-04

This report has been reviewed by EOARD and is releasable to the National Technical Information Service (NTIS). At NTIS it will be releasable to the general public, including foreign nations.

This technical report has been reviewed and is approved for publication.



OWEN R. COTE'
Chief, Geophysics and Space



FRED T. GILLIAM, Lt Col, USAF
Chief Scientist

SECURITY CLASSIFICATION OF THIS PAGE

REPORT DOCUMENTATION PAGE				Form Approved OMB No. 0704-0188	
1a. REPORT SECURITY CLASSIFICATION UNCLASSIFIED			1b. RESTRICTIVE MARKINGS		
2a. SECURITY CLASSIFICATION AUTHORITY			3. DISTRIBUTION/AVAILABILITY OF REPORT APPROVED FOR PUBLIC RELEASE		
2b. DECLASSIFICATION/DOWNGRADING SCHEDULE			DISTRIBUTION UNLIMITED		
4. PERFORMING ORGANIZATION REPORT NUMBER(S) AFOSR-87-0322-3			5. MONITORING ORGANIZATION REPORT NUMBER(S) EOARD-TR-91-04		
6a. NAME OF PERFORMING ORGANIZATION UNIVERSITY OF LEICESTER		6b. OFFICE SYMBOL (if applicable)	7a. NAME OF MONITORING ORGANIZATION EOARD		
6c. ADDRESS (City, State, and ZIP Code) Department of Physics, University of Leicester, Leicester LE1 7RH, UK			7b. ADDRESS (City, State, and ZIP Code) 223/231 Old Marylebone Road LONDON NW1 5TH		
8a. NAME OF FUNDING/SPONSORING ORGANIZATION EOARD		8b. OFFICE SYMBOL (if applicable)	9. PROCUREMENT INSTRUMENT IDENTIFICATION NUMBER AFOSR-87-0322		
8c. ADDRESS (City, State, and ZIP Code) 223/231 Old Marylebone Road LONDON NW1 5TH			10. SOURCE OF FUNDING NUMBERS		
			PROGRAM ELEMENT NO	PROJECT NO	TASK NO
					WORK UNIT ACCESSION NO
11. TITLE (Include Security Classification) STUDIES OF PLASMA IRREGULARITIES AND CONVECTION IN THE POLAR IONOSPHERE USING HILAT, SABRE AND EISCAT					
12. PERSONAL AUTHOR(S) JONES, TUDOR BOWDEN: LEICESTER, MARK					
13a. TYPE OF REPORT FINAL		13b. TIME COVERED FROM Aug. 87 TO 31.3.90		14. DATE OF REPORT (Year, Month, Day) 901231	
15. PAGE COUNT					
16. SUPPLEMENTARY NOTATION					
17. COSATI CODES			18. SUBJECT TERMS (Continue on reverse if necessary and identify by block number)		
FIELD	GROUP	SUB-GROUP	SABRE, EISCAT, PLASMA IRREGULARITIES, IONOSPHERIC CONVECTION, INTERPLANETARY MAGNETIC FIELD		
19. ABSTRACT (Continue on reverse if necessary and identify by block number) The average ionospheric convection patterns measured by SABRE as a function of IMF B_z and B_y have been computed. The convection at SABRE geomagnetic latitudes ($\sim 61^\circ - 66^\circ N$) is seen to be stronger during negative B_z . Asymmetries in the convection pattern are detected as a function of B_y . The nightside flow reversal is found to occur at earlier local times for positive B_y . The duration of purely equatorward flow in this reversal region is found to be longer during intervals of negative B_y . Although there are only a few clear examples, the ionospheric convection associated with the morning reversal, ie. the cusp region, is also dependent upon the sign of B_y . A period of anomalous westward flow occurs at the higher latitudes prior to the reversal during positive B_y conditions. continued.....					
20. DISTRIBUTION/AVAILABILITY OF ABSTRACT <input checked="" type="checkbox"/> UNCLASSIFIED/UNLIMITED <input type="checkbox"/> SAME AS RPT. <input type="checkbox"/> DTIC USERS			21. ABSTRACT SECURITY CLASSIFICATION UNCLASSIFIED		
22a. NAME OF RESPONSIBLE INDIVIDUAL OWEN R. COTE			22b. TELEPHONE (Include Area Code) (44 71) 409-4437		22c. OFFICE SYMBOL EOARD/LDG

DD Form 1473, JUN 86

Previous editions are obsolete.

SECURITY CLASSIFICATION OF THIS PAGE

19. continued....

The occurrence of backscatter during the complete interval of SABRE operations was also investigated. Relating the mean daily backscatter power with various interplanetary parameters such as vB_z , v^2B_z and ϵ indicates that the sign of B_z is the most important parameter. The mean power is considerably higher during intervals of southward B_z . There is also a threshold value of ϵ , above which the mean power increases rapidly. Studies of the periodic nature of the backscatter power have indicated that long term periodicities, ~27 days and 13.5 days, were evident during the descending phase of solar cycle 21. However, these periodicities disappear in the ascending phase of solar cycle 22. This behaviour over the whole solar cycle is believed to result from the nature of the recurrent high speed streams and magnetic field sector structure.

A study which attempted to relate the occurrence of E-region irregularities to the location of the F-region trough was undertaken. No clear relationship appears to exist between these two phenomena based upon data from SABRE and EISCAT taken over a 36 month interval.

Finally, the height of the E-region irregularities measured with the SADIE system was investigated. The apparent time variation of the height measured by SADIE can be reproduced by simply computing the phase difference at the two SADIE antennas based upon the variability of the horizontal distribution of irregularities measured by SABRE. The height of the irregularities did appear, however, to be due to the height where the radar wave vector was estimated to be orthogonal to the background magnetic field.

Accession for	
NTIS	ORAD
DTIC	100
U.S. GOVERNMENT	
January 1981	
By	
Dr. J. G. R. R.	
A-1	
DI	AVIATION



Studies of Plasma Irregularities and Convection in the Polar Ionosphere using HILAT, SABRE and EISCAT.

1. Introduction.

The main aim of this study is to provide new insight into the generation, propagation and decay of scintillation producing plasma irregularities in the high latitude ionosphere. Kilometer-scale plasma irregularities in the F-region can cause scintillation phenomena on trans-ionospheric UHF communication links, thus seriously degrading the system performance. It is, therefore, important to understand more fully the generation, motion and decay of these irregularities. The SABRE radar, which measures coherent backscatter from plasma irregularities in the E-region is the principle instrument employed in this study. Data from the EISCAT radar and the extension to the SABRE system, SADIE, are also utilized.

To achieve the aim of this study, three topics were identified for co-ordinated study:

1. The high-latitude plasma convection pattern as a function of latitude and parameters of the interplanetary environment, and its role in the re-distribution of structured plasma within the polar ionosphere.
2. The morphology and dynamics of the mid-latitude ionization trough as a source of scintillation producing irregularities.
3. The morphology and dynamics of the cusp and its role as a source of structured plasma for the high latitude ionosphere.

Two interim reports (*Jones et al.*, 1988, 1989) have described the work undertaken to study the first two of the above topics. This final report reviews the work reported earlier as well as describing in more detail the work undertaken in the final phase of the contract. This last phase concentrated upon a study of the ionospheric convection associated with the cusp and a separate study of the height of irregularities in the E-region.

2. Instrumentation.

The Sweden And Britain Radar-Auroral Experiment, SABRE, (*Nielsen et al.*, 1983) comprises two multi-beam coherent radars. Each radar measures two parameters, the backscatter intensity and the line of sight Doppler velocity of plasma irregularities that propagate in the auroral E-region with a phase velocity related to the electron drift velocity. The SABRE radars are located at Wick, Scotland, and Uppsala, Sweden, and the beam geometry is illustrated in Figure 1. The SABRE Altitude Determining Interferometer Experiment, SADIE, is an

extension of SABRE (Thomas and Jones, 1989) and employs two parallel, horizontal, colinear antennas separated by 200 m. These antennas have an azimuthal beam width of 3.6 degrees and are oriented so as to provide a beam 26.8 degrees east of north, thus overlaying beam five of the Wick radar (Figure 1). By measuring the phase difference of the backscattered radar echoes received at the two antennas, the angle of elevation of the signals may be determined at each range. From this information the mean height at which the radar signals are scattered, within each range cell, may be calculated.

The European Incoherent Scatter facility (EISCAT) comprises a tristatic UHF incoherent radar, with a transmitter/receiver at Tromso, Norway, and receivers at Kiruna, Sweden, and Sodankyla, Finland, together with a monostatic VHF incoherent radar at Tromso (Baron, 1984). Data from the UHF system only will be considered here. EISCAT operates a number of common modes on a routine basis and data from the Common Programme (CP-3) mode are utilised for part of this study.

3. Dependence of Ionospheric Convection and Backscatter Power on Interplanetary Conditions

In the initial phase of this study (Jones *et al.*, 1988), the dependence on interplanetary conditions of the high latitude ionospheric convection pattern deduced by SABRE measurements was investigated. The dependence on various interplanetary parameters of the backscatter power at Wick was also examined. A secondary investigation studied the long term, >1 day, periodicities in the amplitude of the radar backscatter. This latter study also considered how such periodicities would relate to the magnetic field sector structure in the solar wind.

The convection flows estimated by SABRE between the geomagnetic latitudes 62°N and 66°N (the SABRE field of view) are generally weaker, particularly on the dayside, when the IMF B_z component is northward (data not shown, see Jones *et al.*, 1988). This effect is consistent with the reconnection mechanism (Dungey, 1961) for coupling between the solar wind and magnetosphere, which predicts stronger flows and the expansion of the convection pattern for increasingly negative B_z .

The IMF B_y dependence of the statistical convection flow pattern observed by SABRE was also investigated (Figures 2 and 3). The annular plots indicate that the average time of occurrence of the Harang discontinuity in the centre of the SABRE field of view (64°N, geomagnetic) is approximately 2000 UT for positive B_y (Figure 2) and about 1 hour later at 2100 UT for negative B_y (Figure 3). These results support the conclusion of de la Beaujardière *et al.* (1985), who reported Sondrestrom incoherent radar observations of the ionospheric convection over

the invariant latitude range 68°N to 82°N . These results clearly indicated that the effect of the B_y component is not limited to the noon hours and that the convection pattern was not symmetric for opposite signs of the B_y component of IMF. The occurrence of the Harang discontinuity at earlier local times for positive B_y confirms the conclusion of Rodger *et al.* (1984).

One further difference between the nature of the flows measured by SABRE for negative and positive B_y in the region of the Harang discontinuity is the duration of purely equatorward flow. It appears that the flow tends to be more equatorward when B_y is negative (Figure 3), lasting from 2000 - 2200 UT, compared with positive B_y (Figure 2), 1930 - 2030 UT. This implies that the gradient of the discontinuity (defined by its change in latitudinal location with local time) for negative B_y is not only different from that for positive B_y , but also that the two gradients are not mirror images, further supporting the work of de la Beaujardière *et al.* (1985).

A secondary study considered the direct effect of the solar wind on the occurrence of radar backscatter by relating various solar wind parameters to the daily mean of the Wick radar backscatter intensity. In particular the response of the daily mean backscatter intensity to the parameters $-vB_z$, where v is the solar wind velocity and B_z is the North-South component of the IMF (Rostoker *et al.*, 1972), $-v^2B_z$, where v and B_z are the same as before (Murayama *et al.*, 1980) and ϵ (Perreault and Akasofu, 1978) was investigated (Figures 4, 5 and 6 respectively). The daily mean backscatter intensity changes little for negative values of $-vB_z$, corresponding to northward IMF, and then increases almost linearly as the $-vB_z$ parameter becomes increasingly positive (Figure 4), i.e. as the IMF became more southward. The comparison of the radar data with the $-v^2B_z$ parameter (Figure 5) also suggests the existence of a threshold in the coupling parameter above which the backscatter power is increasingly enhanced (as is the scatter of the data) and generally the relationship is very similar to that for $-vB_z$. The dependence of the radar power on ϵ (Figure 6) is again nonlinear, with the mean backscatter power remaining relatively constant until a threshold value of ϵ of about 10^{10} W is exceeded. The importance of the sign of the southward component is demonstrated by plotting the average Wick power against B_z (Figure 7). The backscatter power is approximately constant for positive B_z , while for $B_z < 0$ the power increases rapidly as B_z becomes more negative.

A preliminary study (Jones *et al.*, 1988) also demonstrated the existence of periodic perturbations in the high latitude ionosphere with periodicities of ~ 27 days and ~ 13.5 days. The latter probably arises from a temporally stable two sector heliospheric structure, resulting in the enhancement of kinetic and magnetic parameters of the interplanetary medium twice per solar rotation. A subsequent study (Yeoman *et al.*, 1990) has demonstrated that this periodic behaviour which

was observed in the radar backscatter during the declining phase of solar cycle 21, disappeared at the start of solar cycle 22 (Figure 8). The power at both the 27 day and 13.5 day periodicities decreases considerably just after 1986, which coincides with the start of the ascending phase of solar cycle 22. The behaviour over the complete solar cycle in the backscatter periodicity can be attributed to the evolution of the heliospheric current sheet during the solar cycle. Details of the radar backscatter, IMF and solar wind spectra (Yeoman *et al.*, 1990) indicate that the solar wind velocity is the dominant parameter in determining the backscatter periodicity.

4. Survey of the mid-latitude trough.

In the second phase of the study (Jones *et al.*, 1989) a statistical investigation of the mid-latitude F-region trough was undertaken to determine if E-region backscatter is more likely to occur when the trough is within the SABRE field of view. A study of the relationship between the latitude of the trough minimum and the latitude of radar backscatter was also undertaken. A more detailed case study of the F-region trough dynamics based upon data from three incoherent scatter radars, EISCAT, Sondre Stromfjord and Millstone Hill, was also reported.

The mid-latitude trough is a region of unusually low electron concentration in the F-region which occurs just equatorward of the auroral oval (see Moffett and Quegan, 1983 for a review). It follows that there are strong gradients in electron concentration, particularly at the poleward edge of the trough, both in the F-region and in the E-region due to particle precipitation, and these gradients may be unstable to the formation of plasma irregularities. The EISCAT CP-3 experiment is designed to provide a latitudinal scan through the ionosphere approximately along a magnetic meridian. The scan time is 26 minutes, with each scan starting on the hour and at 30 minutes past the hour. The scan consists of a number, typically 17, of antenna pointing positions, 16 of which follow approximately the magnetic meridian which passes through Tromsø and Kiruna. At each position, line of sight data are taken at Tromsø with range resolution dependent upon the pulse length and the remote site beams intersect the Tromsø beam at a common height, typically 275 kms, for each scan position. This allows the tri-static ion velocity to be calculated in the F-region. The line of sight data from Tromsø provide information on electron density, electron temperature and ion temperature (see Beynon and Williams, 1978 for a review of the incoherent scatter technique). At 275 kms altitude, the scan covers a geographic range from 64 °N to 75 °N (approximately 61 - 72 °N magnetic latitude). CP-3 provides a data set which can be employed in a morphological study of the main F-region trough during intervals of measurements of irregularities with SABRE, since the EISCAT scan covers a range of latitudes over which the trough is expected to occur in the pre-midnight sector (Moffett and

Quegan, 1983).

In this study, three years of CP-3 data, from 17 January 1984 to 11 November 1986, have been surveyed for features of the trough. This was undertaken by studying summary plots of electron concentration, N_e , and the tri-static ion velocities, v_i , at 275 km altitude, together with the range corrected power profile, PP, measurements at 110 km altitude. The trough was initially identified in a plot of N_e as a function of latitude and time at 275 km and auroral features in a plot of PP as a function of latitude and time at 110 km. During the interval mentioned above there were 54 runs of CP-3 and during 36 of these the trough was identified (Figure 9, upper panel). As expected (Moffett and Quegan, 1983), the trough occurred during the winter and equinoctial months but not during the summer months (May - July).

A comparison of times when the trough was detected by EISCAT with times when the Wick radar received coherent backscatter indicated a high percentage of coincidence. In 26 cases out of the 36 intervals when the trough was observed coherent backscatter also occurred during a part of the local time sector when the trough was observed (Figure 9, lower panel). On another 5 occasions backscatter occurred within 1 hour of the local time of occurrence of the trough (data not shown in Figure 9). However, during the 18 intervals when no trough was observed, there were 12 examples when backscatter occurred during the 12 - 24 UT interval, the interval when the trough is typically observed with the CP-3 experiment. This suggests that the simple comparison outlined above does not provide sufficient information on the coincidence of trough and auroral backscatter, since the percentage occurrence of trough and backscatter, 72%, is not significantly different from the percentage of times when backscatter occurred for part of the 12 - 24 UT interval when CP-3 was running and no trough occurred.

A further study was undertaken which compared the latitude of the trough minimum, a characteristic of the trough which is both easily defined and relatively easily identified from the CP-3 data, with three parameters of the coherent backscatter, the latitudes of the poleward and equatorward borders and the latitude of the peak backscatter intensity. If E-region backscatter were preferentially generated at some region of the trough then we would expect a consistent picture to emerge from this study. However, not one of the backscatter parameters was found consistently to relate to the trough minimum latitude. Two examples of the comparisons are given in Figure 10 to illustrate the lack of consistency between backscatter latitude and trough minimum latitude. On 24 September 1986, Wick backscatter began at ~ 1800 UT (~ 1900 LT). At this local time the trough, as measured by EISCAT, occurred between ~ 66 °N magnetic latitude and ~ 63 °N magnetic latitude (Figure 10, upper panel, open circles). The peak backscatter intensity (squares) initially occurred at a latitude of approximately 64 °N and moved equatorward over the next hour by ~ 1 degree, during which time it remained very close to the trough minimum. The

backscatter exhibited a poleward border (Figure 10, upper panel, crosses) which also moved equatorward during the interval. The equatorward border remained at $\sim 62.5^\circ\text{N}$ magnetic latitude, very close to the lowest latitude of the field of view. Compare these observations with those of 26 September 1986 (Figure 10, lower panel). The onset of backscatter on this day occurred at ~ 1600 UT (~ 1700 LT), when the trough was between 67°N and 66.5°N magnetic latitude. The peak backscatter (squares) was some 3 degrees equatorward of the trough position, apart from the last 15 minutes or so of the interval, when the trough minimum had moved equatorward. Neither the poleward or equatorward borders moved in the same manner as the trough. These two examples demonstrate that the latitude of the minimum N_e in the F-region trough is not consistently related to the latitude of auroral backscatter and leads to the conclusion that it is not possible to determine if there is preferential generation of irregularities in the E-region associated with the F-region trough.

5. SABRE Observations of the Cusp

In the final phase of the study two separate investigations were undertaken. The first investigated the ionospheric convection associated with the cusp and the second the height of E-region irregularities which cause auroral backscatter. Observations of the ionospheric convection in the vicinity of the morning flow reversal, which is the ionospheric footprint of the magnetospheric cusp, are of considerable interest since this is a region of direct coupling between the geomagnetic field and the IMF. In this study the cusp was defined as the region where sunward dayside convection flow turns anti-sunward to flow across the polar cap. Because of the displacement of the auroral oval towards the nightside, observations of cusp associated flows by SABRE are extremely rare. Under quiet conditions the cusp is located at about 76°N geomagnetic latitude (Burch, 1979), whereas SABRE covers the geomagnetic latitude range 61.5°N to 66.5°N . It is generally accepted that the cusp does shift equatorward during times of southward IMF (e.g. Burch, 1979; Meng, 1983; Sandholt *et al.*, 1985) due to the increased rate of dayside merging at the dayside magnetopause between IMF and the geomagnetic field. Hence, strong convection flows are expected within the SABRE field of view in the morning local time sector (0600 - 1200 MLT) only during disturbed geomagnetic conditions.

During the lifetime of dual radar operations of SABRE, there were 9 days during which the morning convection reversal was identified in the SABRE field of view. These days are listed in Table 1, together with an estimate of the time of the reversal from east to west (T_{MR}), measured in the middle of the viewing area at a geomagnetic latitude of 63°N . If the reversal is ill defined or there is a loss of backscatter between the end of eastward flow and the start of westward flow, a time interval indicating the uncertainty in the time interval (ΔT_{MR}) is quoted.

Also included in Table 1 are the values of Kp, Dst and, where available the AE index. The generally very large values of these geomagnetic indices are indicative of the unusually disturbed conditions required for SABRE to observe cusp flows.

Also presented in Table 1 is the inferred polarity of the IMF based upon magnetograms from Vostok, Antarctica (Mansurov, 1969; Svalgaard, 1973). An IMF polarity denoted A (away from the Sun) corresponds to a positive B_y component, while T (towards the Sun) indicates a negative B_y component. The abbreviations AT and TA indicate that the inferred polarity displayed a clear change during the 0-12 hour UT interval from away to toward or toward to away respectively. The inferred IMF polarity is used here because of the lack of spacecraft data for these intervals. ISEE-3 measurements are available for four of the intervals, but for two of them the spacecraft is not only downstream of the Earth but also close to the geomagnetic tail. For these last two intervals identifying the solar wind is difficult, in particular distinguishing when the spacecraft is in the solar wind from when it is in the magnetosheath. Note that there is no apparent dependence of the local time of the reversal in flow on the inferred direction of the IMF.

A SABRE Range Time Velocity (RTV) plot for the interval from 0745 to 1015 UT is presented in Figure 11. This figure illustrates the time development of the convection flow as a function of latitude observed by SABRE with an integration time of 3 minutes and averaged over a 2 degree wide longitudinal strip between 5°E and 7°E . The vectors depict estimates of the flow magnitudes and flow directions. The essential feature of the pattern observed by SABRE is the rotation at 0930 UT of the eastward flows associated with the westward electrojet to eastward flows associated with the eastward electrojet. Prior to the reversal, between 0830 and 0925 UT, the eastward flow is interrupted by a region of anomalous westward flow poleward of about 66°N geographic latitude. The westward flow incursion is terminated by a region of north-east directed flow associated with the main east-west flow reversal, which occupies the entire latitudinal extent of the viewing area. The temporal location of the eastern boundary or trailing edge of the wedge of westward flow exhibits a latitudinal variation. The boundary is observed at 0905 UT for a latitude of 66°N , but not until 0925 UT for a latitude of 62°N .

Measurements of the IMF by ISEE-3 which was at an approximate location of $X=197$, $Y=-85$ and $Z = 1 R_E$ are given in Figure 12 for the interval 0000 - 1200 UT. Except for a large but brief enhancement shortly before 0900 UT, the average solar wind flow velocity between 0700 UT and 0930 UT was 600 kms-1. Assuming that the solar wind remains uniform from the spacecraft to the Earth then the time delay for changes to reach the Earth from the satellite is approximately 35 minutes. This calculation also makes the assumption that the magnetic field is constant in a plane which is perpendicular to the Sun-earth line. This last

assumption is important because of the large displacement of the spacecraft in the Y direction in this particular case. If the plane is not perpendicular to the Sun-Earth line then large errors, of up to 20 minutes or so, in the time delay could result (Lester *et al.*, 1990). Taking the delay of 35 minutes, the period of interest at ISEE-3 corresponding to the interval of convection produced in Figure 11 is 0710 UT to 0940 UT. Apart from a 9 minute interval from 0723 - 0732 UT, the IMF B_y component was positive throughout the interval of interest. Note that at about 0800 UT the convection flow becomes north-east directed and interrupts the incursion of westward flow which started originally at 0754 UT. Whether this north-east flow, which lasts for some 30 minutes, is related to the change in B_y is difficult to tell with the large errors involved in the calculation of the delay from the spacecraft to the magnetosphere. The duration of the north-east flow is however considerably larger than the interval of negative B_y .

Two other examples of cusp associated convection during intervals of either measured or inferred positive B_y occurred on 16 November 1984 and 2 March 1983, at ~0730 UT and at ~0630 UT respectively. On both days the convection exhibited an incursion of westward flow similar to that illustrated in Figure 11 lasting for some 30 minutes on 16 November and 45 minutes on 2 March. Of these two intervals there were only IMF data available for the second, when ISEE-3 was located at $X=-195$, $Y=48$, $Z=-8R_E$ and the solar wind velocity was ~ 400 ms^{-1} . Making the same assumptions as above gives a time delay of -50 minutes. The IMF data available for March 2 indicate that the B_y component was positive from 0600 UT until 0845 UT, equivalent to ~0510 UT to 0755 UT at the Earth.

Cusp flows observed on 5 February when the inferred polarity was consistent with negative B_y (Figure 13) are less complex than the flows associated with positive B_y . The flow reversal occurred at about 0810 UT with no obvious latitudinal dependence and the time interval from 0730 UT to 0830 UT, in the vicinity of the discontinuity, is characterised by weak flows. The absence of any pre-reversal westward flow incursion is consistent with the inferred B_y polarity, which was negative for the 0600 to 1200 UT. Similar observations of cusp associated ionospheric flows were made on 7 August 1982 when again the inferred B_y polarity was negative.

While increasingly negative B_z generally produces equatorward expansions of the large-scale convection pattern, the B_y component of the IMF is expected to cause dawn-dusk asymmetries in the convection pattern (Cowley, 1982). Figure 14 illustrates a schematic representation of the dayside convection for positive, zero and negative B_y , incorporating simple diagrams of depicting the expected flow directions in the SABRE viewing area in the cusp region. Naturally the directions of the flows are different depending upon the sign of B_y . The evolution of the ionospheric convection that SABRE would measure as the radar field of view rotated beneath a temporally stable convection pattern for

positive B_y is illustrated in Figure 15. As the field of view moves from position 1 to position 2, westward (antisunward) flows should move equatorwards across the field of view. At the boundary between the dawn and dusk cells (position 3) the flows would be predominantly poleward, but with a westward component. At position 4 the flow should have become predominantly westward (sunward) after moving to a time later than the that of the reversal.

A sequence of SABRE spatial plots from 6 September 1982 (Figure 16) are in broad agreement with this scenario. There are some discrepancies, however, when flow changes occur too rapidly to be explained by rotation beneath a fixed pattern. An example is the change between 0833 UT and 0839 UT (Figure 16) when initially westward flow occupies just a small area at the north of the field of view but by 0839 UT covers almost half of the field of view. Such a rapid equatorward move of the westward flow is more likely to be due to temporal change in the coupling conditions between the magnetosphere and the solar wind. There is, however, no evidence for any significant change in either the IMF or the solar wind velocity or density at about 0800 UT.

Finally the lack of a similar signature during negative B_y conditions is probably due to the fact that the convection pattern has not expanded far enough equatorward. The poor statistics do not enable us to test this conclusion.

6. Interferometer Study of E-Region Irregularities

The characteristics of irregularities which generate coherent radar backscatter are critically dependent upon the height at which the irregularities occur (Robinson, 1986). One such characteristic is the irregularity phase velocity which is equivalent to the Doppler velocity measured by the radar. Hence, it is important to determine the height distribution of the irregularities causing the radar backscatter. The SABRE Altitude Determining Interferometer Experiment (SADIE) was deployed to investigate this particular problem. Initial results from SADIE (Thomas and Jones, 1989) demonstrated that the apparent height of the irregularities could on occasion be highly variable (Figure 17). A more detailed examination of the SADIE data set has been undertaken in order to fully understand the nature of this variability.

As mentioned earlier, SADIE is an extension to the SABRE system consisting of two parallel, horizontal, colinear antennas separated by 200 m. The phase difference between the two SADIE antennas of the received signals can then be used to calculate the height at which the irregularities occur (Thomas and Jones, 1989). The antenna beam width is 3.6 degrees and the antennas are oriented such that the beam overlaps beam 5 of SABRE (Figure 1). The operation of the two systems, SABRE and SADIE, was simultaneous to check that the phase difference measured by SADIE was not influenced by any horizontal distribution

of the irregularities.

In fact the finite radar beam width and the intensity distribution in azimuth (i.e. horizontal distribution) can introduce an error into the height determination due to the effective path difference

$$\Delta d_A = \frac{1}{W} \int_{\phi_{min}}^{\phi_{max}} I(\phi) A(\phi) D d(\phi) d\phi \quad (1)$$

where

$$W = \int_{\phi_{min}}^{\phi_{max}} A(\phi) I(\phi) d\phi \quad (2)$$

$I(\phi)$ is the linear backscatter intensity as determined by the eight horizontally distributed SABRE beams and $A(\phi)$ is the horizontal antenna sensitivity function of the interferometer approximated by

$$A(\phi) = S(\phi) \frac{\sin^2 y}{y^2} \quad (3)$$

with

$$y = \pi D_0 / \sin \phi \quad (4)$$

and

$$S(\phi) = 1 \text{ for } \phi \leq 4.8^\circ \quad (5a)$$

or

$$S(\phi) = 0.2 \text{ for } \phi > 4.8^\circ \quad (5b)$$

For the wavelength of SABRE and SADIE, $\lambda=1.958\text{m}$, a value of $D_0=24\text{m}$ was found to match the actual antenna sensitivity function best. The factor $S(\phi)$ was introduced to account for the suppressed sidelobe sensitivity. It should be noted that equation 1 assumes an incoherent superposition of the backscatter from different regions, i.e. it neglects the additional phase changes introduced by adding waves of different amplitudes and/or initial phase together. This assumption is justified for two reasons. The first is that the long integration time (20 s) compared to irregularity life time acts as an averaging process over the location of the scatterers (i.e. irregularities) which can change because of thermal and systematic motions by several hundred meters and thus by many wavelengths within the integration time. Hence the time integrated

contributions from different azimuth angles should therefore be completely uncorrelated in phase. Secondly the dimensions of the receiving antenna (30 m) are large compared with the wavelength (2 m) and thus produce a further spatial averaging.

Because only eight beams (each separated by 3.6 degrees) are available to determine the horizontal intensity pattern, equation 1 reduces to a sum over these 8 directions. Various types of interpolation have been tried in order to achieve a better approximation to the integrand, showing little effect on the value of the integral. In the calculation reproduced here 65 directions and an exponential interpolation between 8 beam centre directions, to which the measured intensities were assigned, have been utilised.

The path difference was determined for a given range along the SADIE beam assuming an azimuth independent backscatter height H , which was chosen to be the height of orthogonality of the radio wave with the magnetic field (115 km for 900 km range and 110 km for 705 km range). The average azimuthal path difference obtained from equation 1 was then formally used in the interferometer equation in the manner of the phase difference between the two SADIE antennas. Figures 18 and 19 illustrate the apparent height variations for the two intervals in Figure 17. The heights obtained by the experimental phase measurements are indicated by squares. The apparent height error due to the horizontal intensity distribution is given by two fully drawn curves. The thin curve was produced using the original intensities; the thick curve was produced using an amplification factor for the intensities. In both figures this amplification factor is of order 12. With the horizontal intensity distribution manipulated in this manner the interferometer results (the squares) can be almost exactly reproduced. There is an exact correlation between the phase of the fluctuation detected with the interferometer and the modelled phase changes expected from the variations in the horizontal intensity distribution, though the amplitude of the latter is about one order of magnitude smaller.

It seems, therefore, that the apparent variations in height measured by SADIE (Figure 17) are in fact not real variations but simply due to the effect of the horizontal intensity distribution of the irregularities which cause the radar backscatter. This is an important result, both in terms of the system and in terms of the distribution of irregularities. Clearly the distribution of irregularities within the radar field of view is not always homogeneous in the horizontal plane, even when there appears to be considerable backscatter over the whole field of view. The question now arises as to the nature of the inhomogeneity of the horizontal distribution of the irregularities, especially within each of the radar beams. This cannot be answered simply with the existing systems. The SADIE system cannot unambiguously determine the height of the irregularities, although there is evidence that the apparent height does come from very close to the estimated orthogonality height. Figure 20 illustrates four examples of the mean variation of estimated irregularity height by SADIE as a function of range.

Also plotted on each panel of Figure 20 is the estimated height at which orthogonality between the radar wave vector and the magnetic field occurs. There are two notable effects. Firstly the estimated height increases with increasing range and secondly the estimated height tends to be higher than the orthogonality height. This apparent divergence from the orthogonality height can be explained simply in terms of the geometrical increase of the linear azimuthal distance from the interferometer axis as the range increases.

7. Summary.

The results of the three phases of this study, together with the investigation of the altitude dependence of irregularities can now be summarised. There is a clear dependence of the ionospheric convection upon the north-south component of the IMF, B_z , which results in an expanded convection pattern during intervals of southward B_z and weaker convection at SABRE latitudes during northward B_z . There is also clear evidence of an asymmetry in the convection pattern introduced by the sign of the azimuthal component of the IMF, B_y . In particular this asymmetry is identified in the nightside in the region of the Harang Discontinuity which occurs at earlier local times for positive B_y . Furthermore, the structure of the flows associated with the evening flow reversal tends to differ for different B_y conditions. The duration of purely equatorward flow in the average conditions lasts longer for negative B_y than for positive B_y .

An investigation of the occurrence of radar backscatter and its dependence on interplanetary conditions revealed that the sign of the B_z component was again most important. Several different interplanetary parameters were tested, including $-vB_z$, $-v^2B_z$ and ϵ , but it was clear that the sign of B_z was the significant contributory factor to the occurrence of irregularities within the SABRE field of view. A subsequent study noted that long term periodicities, ~ 27 days and 13.5 days, existed in the radar backscatter data at the time of the descending phase of the solar cycle. A later study demonstrated that these periodicities disappeared during the ascending phase of the following solar cycle. The disappearance is attributed to the change in the recurrent nature of high speed streams and sector structure during the ascending phase of the solar cycle.

A statistical study relating the occurrence of the F-region trough and E-region auroral backscatter suggested at least a coincidence between these two features for $\sim 70\%$ of the time. However, this is probably not significantly better than the normal occurrence of auroral backscatter when observations of electron density profiles were also made. Furthermore, a study of the latitude of backscatter peak intensity and the poleward and equatorward edges to the backscatter proved inconclusive with regard to a relationship to the trough minimum. The

inconsistency of the results was illustrated with two examples. A detailed case study of the trough on 4 days suggests that in fact any relationship is due to similar formation mechanisms, rather than preferential generation. The trough formation mechanism within the post noon sector and one of the irregularity generation mechanisms, i.e. the two-stream instability (*Fejer and Kelley, 1980*) are both related to enhanced ion convection. The F-region trough may still be an important location for the generation of irregularities in the F-region ionosphere which would affect HF coherent radars and cause F-region scintillation.

In the last phase of the study an investigation of the convection near the cusp was undertaken. There are few observations of the cusp associated convection flows by the SABRE radar because of the radars relatively low latitude. However, those events that have been observed indicate clear differences between the flows associated with negative B_y , when the reversal appears to be a simple eastward to westward flow change, compared to positive B_y , when there is an incursion of anomalous westward flow prior to the reversal. This difference is again attributed to the asymmetry in the convection associated with different B_y conditions.

A final study of the height of the plasma irregularities in the E-region measured by SADIE demonstrated that the apparent height variations with time could be attributed to variations of the horizontal backscatter distribution. The height appears to be close to the estimated height of the orthogonality between the radar wave vector and the geomagnetic field.

References.

- Baron, M., The EISCAT Facility, *J. Atmos. Terr. Phys.*, **46**, 469 - 472, 1984.
- Beynon, W.J.G. and P.J.S. Williams, Incoherent Scatter of Radio Waves from the Ionosphere, *Rep. Prog. Phys.*, **41**, 909, 1978.
- Burch, J.L., Effects of the Interplanetary Magnetic Field on the Auroral Oval and Plasmopause, *Space Sci. Rev.*, **23**, 449 - 464, 1979.
- Cowley, S.W.H., Magnetospheric and Ionospheric Flow and the Interplanetary Magnetic Field, in *The Physical Basis of the Ionosphere in the Solar-Terrestrial System*, p 4-1, AGARD, Neuilly-sur-Seine, France, 1982.
- de la Beaujardière, O., V.B. Wickwar and J.D. Kelley, Effect of the Interplanetary Magnetic Field Y component on the High-Latitude Nightside Convection, *Geophys. Res. Lett.*, **12**, 461 - 464, 1985.
- Dungey, J.W., Interplanetary Magnetic Field and the Auroral Zones, *Phys. Rev. Letts.*, **6**, 47 - 48, 1961.
- Fejer, B.G. and M.C. Kelley, Ionospheric Irregularities, *Rev. Geophys. Space Phys.*, **18**, 401 - 454, 1980.
- Jones, T.B., M.D. Burrage, and M. Lester, Studies of Plasma Irregularities and Convection in the Polar Ionosphere using HILAT, SABRE and EISCAT, *Interim Report, AFOSR-87-0322*, May 1988.
- Jones, T.B., M. Lester and A.J. Wilkinson, Studies of Plasma Irregularities and Convection in the Polar Ionosphere using HILAT, SABRE and EISCAT, *Interim Report, AFOSR-87-0322*, August 1989.
- Lester, M., M.P. Freeman, D.J. Southwood, J.A. Waldock and H.J. Singer, A Study of the Relationship Between Interplanetary Parameters and Large Displacements of the Nightside Polar Cap Boundary, *J. Geophys. Res.*, **95**, 12,123 - 12,145, 1990.
- Mansurov, S.M., New Evidence of a Relationship Between Magnetic Fields in Space and on Earth, *Geomag., Aeron.*, **9**, 622 - 623, 1969.
- Meng, C.-I., Case Studies of the Storm Time Variation of the Polar Cusp, *J. Geophys. Res.*, **88**, 137 - 149, 1983.
- Moffett, R.J. and S. Quegan, The Mid-Latitude Trough in the Electron Concentration of the Ionospheric F-layer: A Review of Observations and Modelling, *J. Atmos. Terr. Phys.*, **45**, 315 - 343, 1983.
- Murayama, T., T. Aoki, H. Nakai and K. Hakamda, Empirical Formula to Relate the Auroral Electrojet Intensity with Interplanetary Parameters, *Planet. Space*

- Sci.*, **28**, 803 - 814, 1980.
- Nielsen, E., W. Guttler, E.C. Thomas, C.P. Stewart, T.B. Jones and A. Hedberg, A New Radar Auroral Backscatter Experiment, *Nature*, **304**, 712 - 714, 1983.
- Perreault, P. and S.-I. Akasofu, A Study of Geomagnetic Storms, *Geophys. J. Roy. Astron. Soc.*, **54**, 547 - 573, 1978.
- Robinson, T.R., Towards a Self-Consistent Non-Linear Theory of Radar Auroral Backscatter, *J. Atmos. Terr. Phys.*, **48**, 417 - 422, 1986.
- Rodger, A.S., S.W.H. Cowley, M.J. Brown, M. Pinnock and D.A. Simmons Dawn-Dusk (Y) Component of the Interplanetary Magnetic Field and the Local Time of the Harang Discontinuity, *Planet. Space Sci.*, **32**, 1021 - 1027, 1984.
- Rostoker, G., H.-L. Lam and W.D. Hume, Response Time of the magnetosphere to the Interplanetary Electric Field, *Can. J. Phys.*, **50**, 544 - 547, 1972.
- Sandholt, P.E., A. Egeland, J.A. Holtet, B. Lybekk, K. Svenes, S. Asheim and C.S. Deehr, Large- and Small-Scale Dynamics of the Polar Cusp, *J. Geophys. Res.*, **90**, 4407 - 4414, 1985.
- Svalgaard, L., Polar Cap Magnetic Variations and their Relationship with the Interplanetary Magnetic Sector Structure, *J. Geophys. Res.*, **78**, 2064 - 2078, 1973.
- Thomas, E.C. and T.B. Jones, Height Measurements of VHF Scattering Irregularities in the E-Region, *Proc. Sixth Intl. Conf. Antenn. and Prop., IEE Conf. Pub. 301*, 2.196 - 2.200, 1989.
- Yeoman, T.K., M.D. Burrage, M. Lester, T.R. Robinson and T.B. Jones, Long Term Variation of Radar-auroral Backscatter and the Interplanetary Sector Structure, *J. Geophys. Res.*, **95**, 12,123 - 12,132, 1990.

Figure Captions.

- Figure 1. The beam geometries for the two radars at Wick and Uppsala that constitute SABRE. Beam 5 (counted clockwise from the most northerly directed beam) of the Wick radar corresponds to the SADIE beam.
- Figure 2. The average flows measured by SABRE during positive IMF B_y conditions as a function of UT and geomagnetic latitude. The SABRE data are averaged over 15 minutes intervals.
- Figure 3. A similar plot to Figure 2 for negative IMF B_y conditions.
- Figure 4. The mean Wick power in dB plotted as a function of $-vB_z$ in units of mVm^{-1} where v is the solar wind velocity and B_z is the north/south component of the IMF with positive measured in the north direction. Negative $-vB_z$ means positive B_z . The standard error in the mean value is represented by the error bars. The number of points in each bin is given by the dotted line.
- Figure 5. A similar plot to that in Figure 4 but the mean Wick power is plotted as a function of $-v^2B_z$ in units of $10^6 \text{ nT km}^2 \text{ s}^{-2}$.
- Figure 6. A similar plot to that in Figure 4 but the mean Wick power is plotted as a function of $\log_{10} \epsilon$.
- Figure 7. A similar plot to that in Figure 4 but the mean Wick power is plotted as a function of the north/south component of the IMF, B_z .
- Figure 8. A plot of the power in 4 frequency bins, $0.034 - 0.042 \text{ days}^{-1}$ (full line), $0.068 - 0.076 \text{ days}^{-1}$ (long dashed line), $0.108 - 0.116 \text{ days}^{-1}$ (dot/dash line) and $0.144 - 0.152 \text{ days}^{-1}$ (short dash line), as a function of time. The frequency spectrum is calculated over a period of 200 days with an overlap of 100 days. The two lower frequency bins, equivalent to the full line and the long dashed line, represent the 27 days and 13.5 days periods.
- Figure 9. The occurrence frequency of the F-region trough observed by the EISCAT CP-3 programme for the three year interval 1984 - 1986. The upper panel gives the distribution of CP-3 observations and trough occurrence. The lower panel gives the trough occurrence and the occurrence of those intervals when backscatter was also observed by SABRE.
- Figure 10. The variation of the latitude of the trough minimum with local time together with the latitude of the peak backscatter intensity the latitude

of the equatorward border of the backscatter (EB) and the poleward border of the backscatter (PB). The upper panel is for 24 September and the lower panel for 26 September.

- Figure 11. SABRE Range Time Velocity (RTV) plot for the interval 0745 to 1015 UT on 6 September (Day 249) 1982
- Figure 12. ISEE-3 measurements of the solar wind flow speed and density (top two panels) and the GSE components X, Y and Z, of the IMF for the period 0000 - 1200 UT on 6 September 1982.
- Figure 13. SABRE Range Time Velocity (RTV) plot for the interval 0630 - 0900 UT on 5 February.
- Figure 14. Schematic representation of the predicted large scale dayside convection patterns for positive, zero and negative B_y , incorporating simple diagrams that depict the expected flow directions in the SABRE viewing area in the vicinity of the cusp.
- Figure 15. Schematic representation of the predicted large scale dayside convection pattern for positive B_y , indicating the successive positions of the SABRE viewing area as the Earth rotates under the pattern. The dashed line denotes the polar cap boundary.
- Figure 16. A sequence of SABRE spatial plots for the morning of 6 September 1982.
- Figure 17. Apparent height of E-region plasma irregularities on (a) quiet day and (b) disturbed day.
- Figure 18. Phase fluctuations of auroral backscatter for Day 268, 1987, 14 - 15 UT at a range of 705 km, formally transformed into height variations. Squares represent the SADIE interferometer data. The fully drawn curve shows the modelled effect due to the horizontal intensity pattern (thin line original SABRE intensity; thick line with an intensity distribution which has been amplified).
- Figure 19. A similar plot to Figure 18 for Day 337, 1987 1515 - 1615 UT and a range 900 km.
- Figure 20. Time averaged (one hour) range dependence of the apparent height for several dates.

TABLE 1

YEAR	DAY	T _{MR} (UT, hr)	ΔT_{MR} (mins)	Dst (nT)	Kp	AE (nT)	Inf. IMF
1982	219	9:00	60	-137	7+	764	Def. T
1982	249	9:30	<5	-236	8+	1036	Def. A
1982	355	8:50	40	-83	5-	204	Def. A
1983	36	8:10	5	-168	7+	650	A T
1983	38	8:40	40	-85	5+	268	Def. T
1983	61	8:20	<5	-149	7	679	T A
1984	321	8:00	<5	-133	7	-	A
1985	118	9:00	<5	-99	7	-	T A
1986	255	7:30	30	-166	7+	-	-

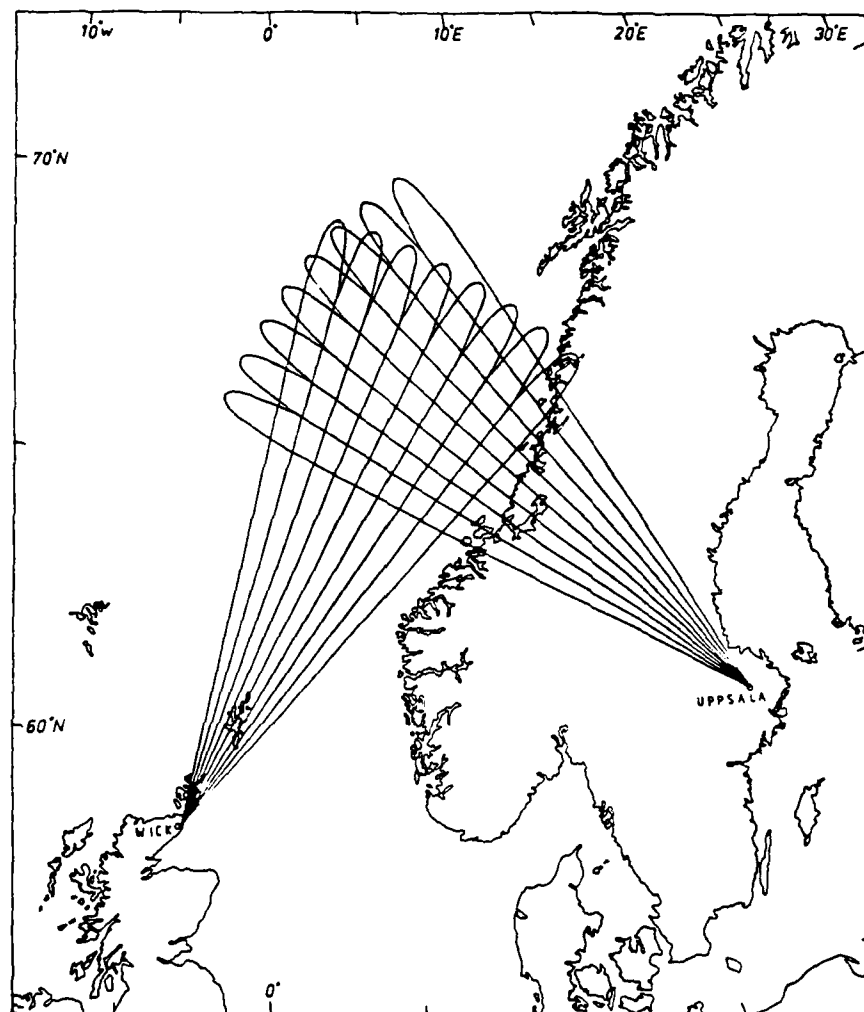


Fig.1

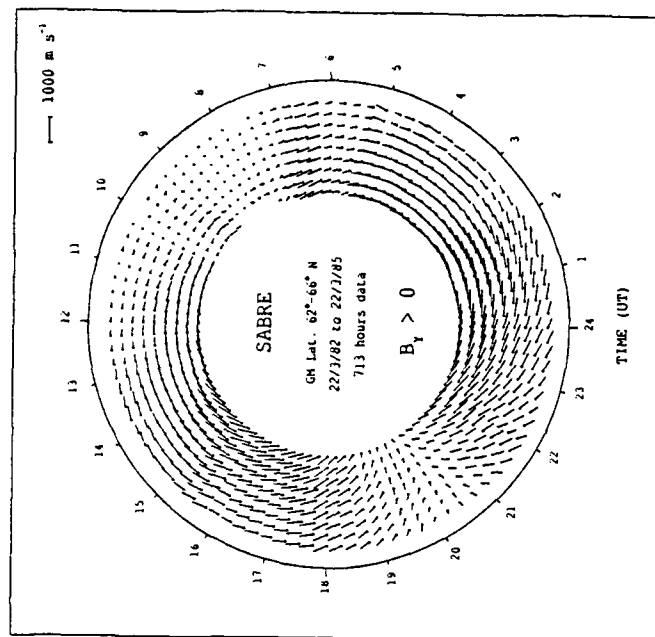


Fig. 2

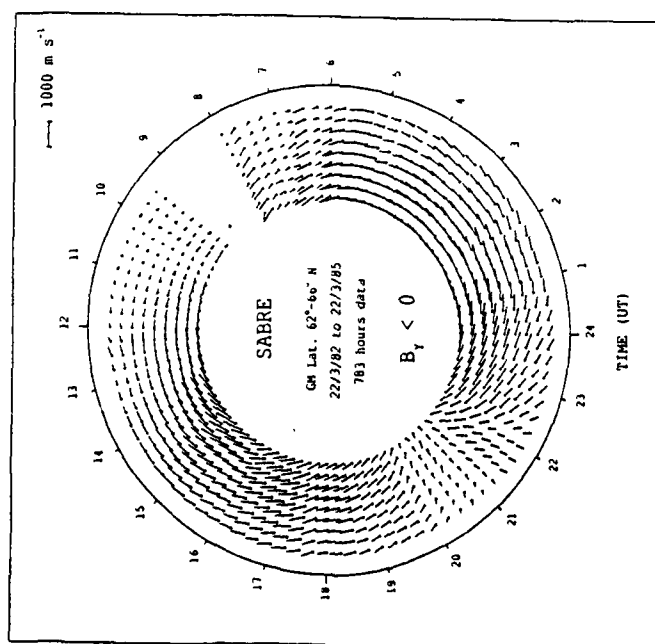


Fig. 3

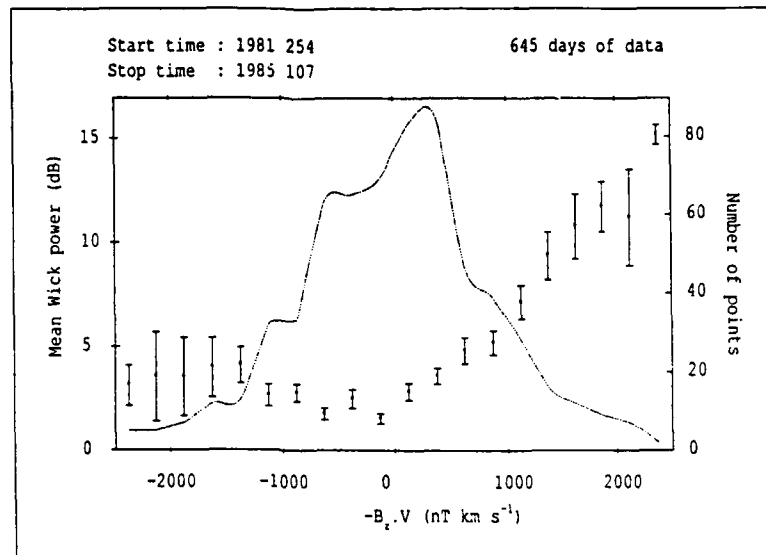


Fig. 4

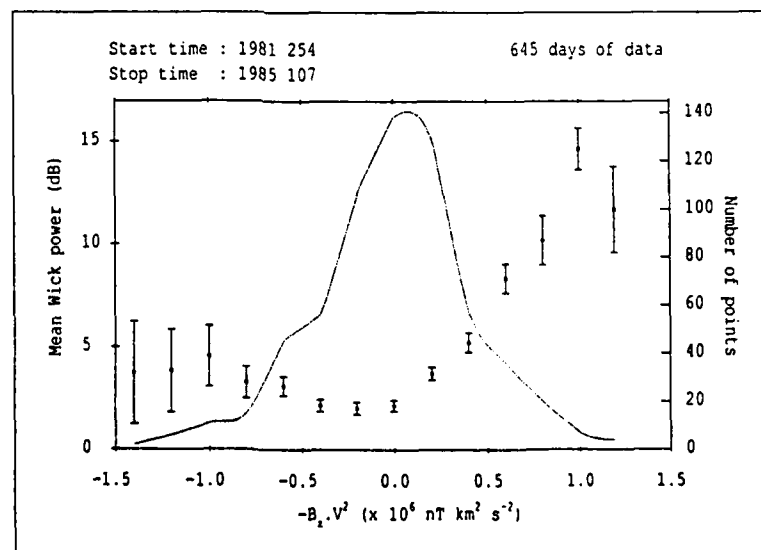


Fig. 5

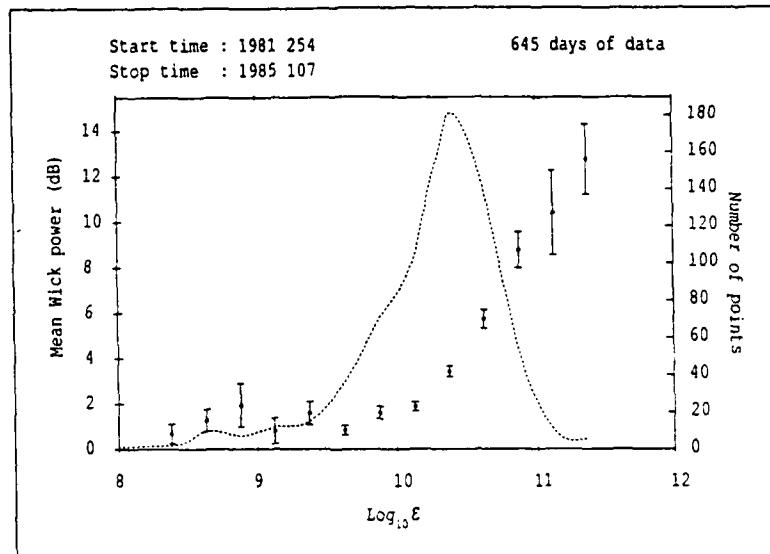


Fig. 6

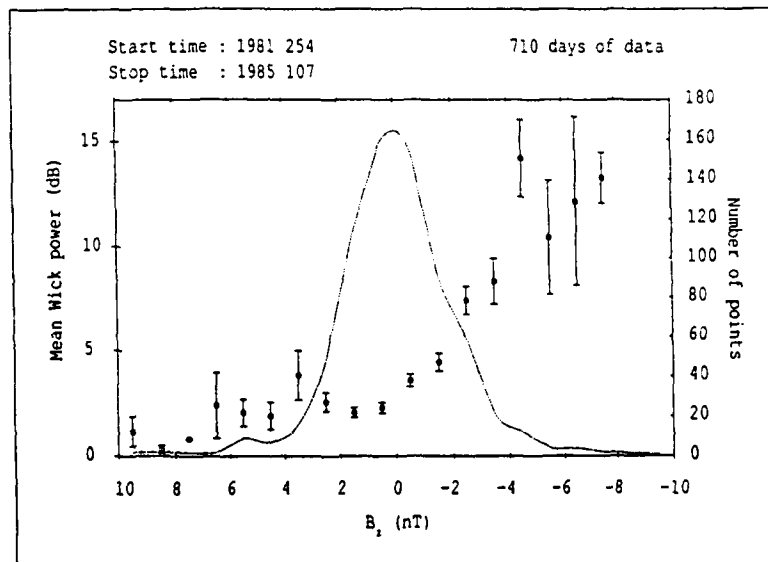


Fig. 7

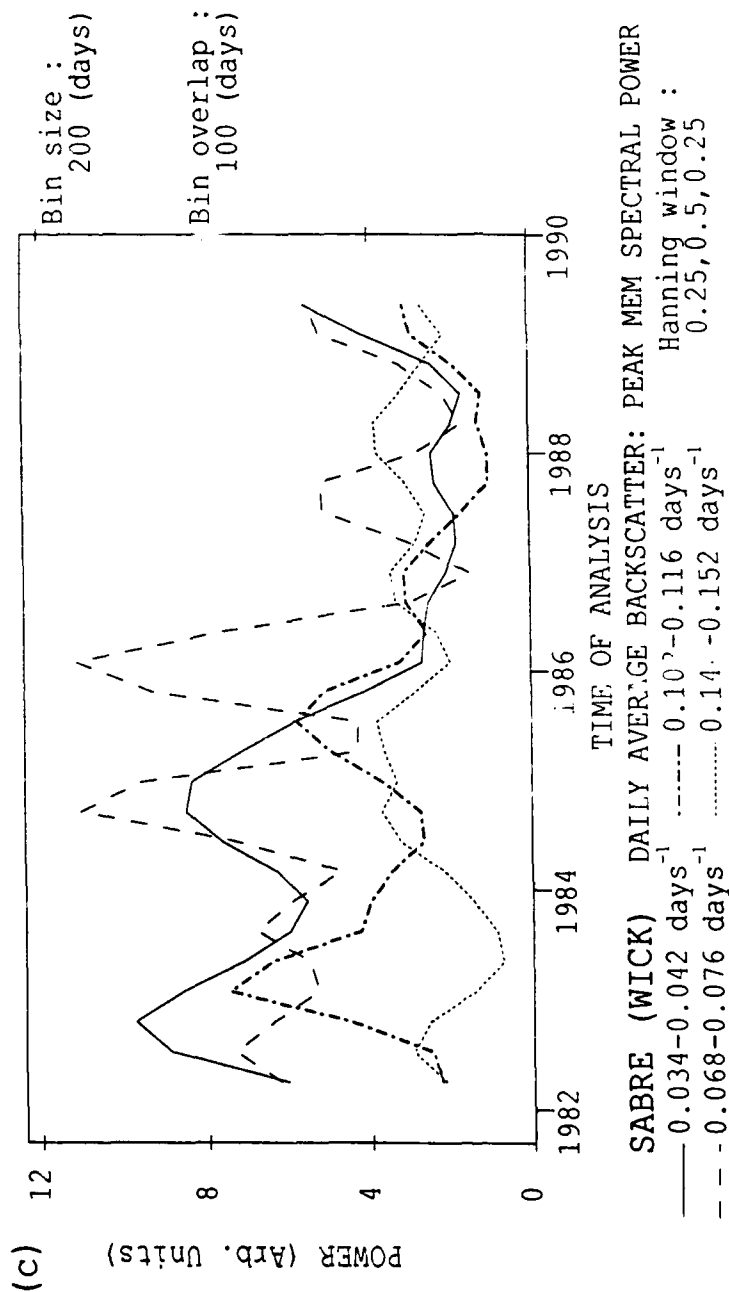


Fig. 8

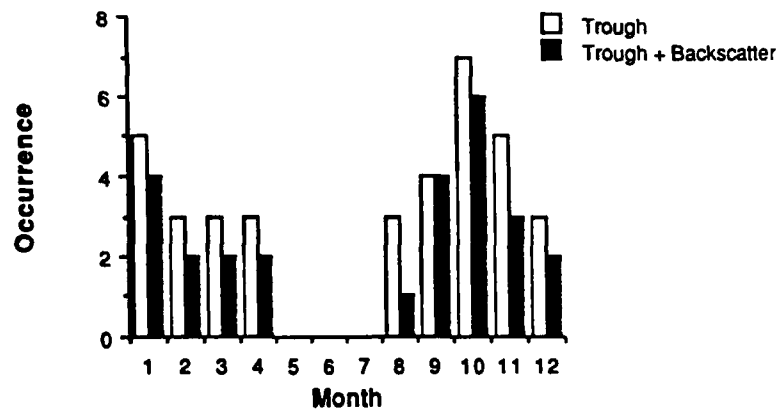
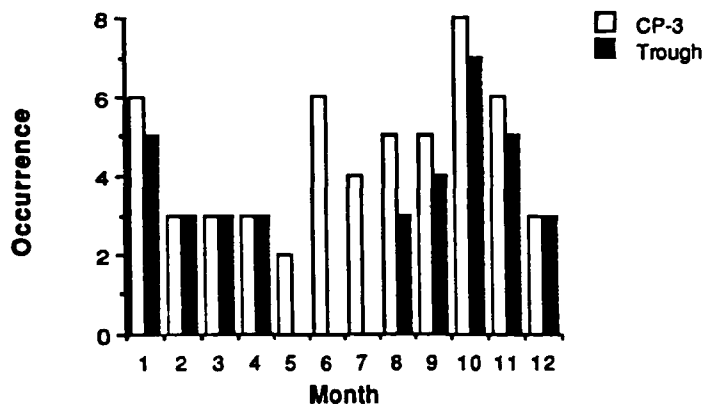


Fig. 5

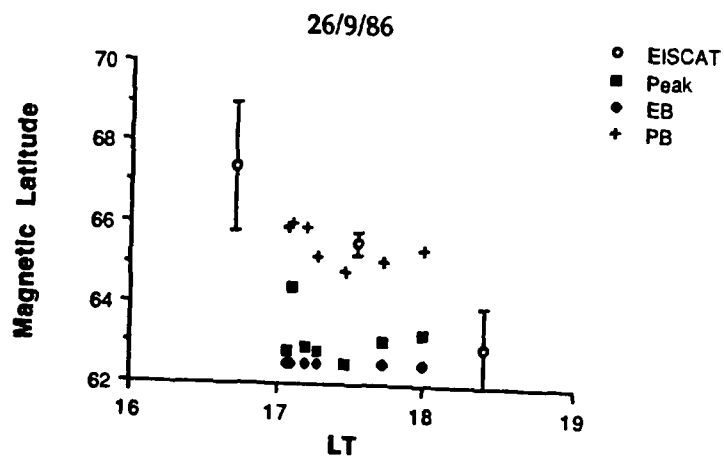
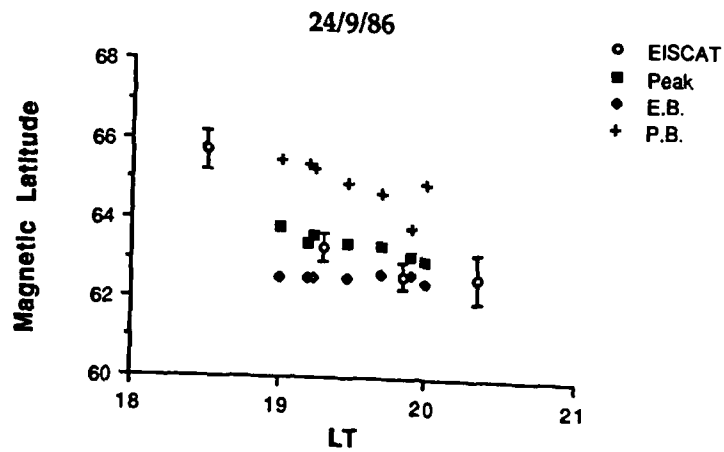


Fig. 10

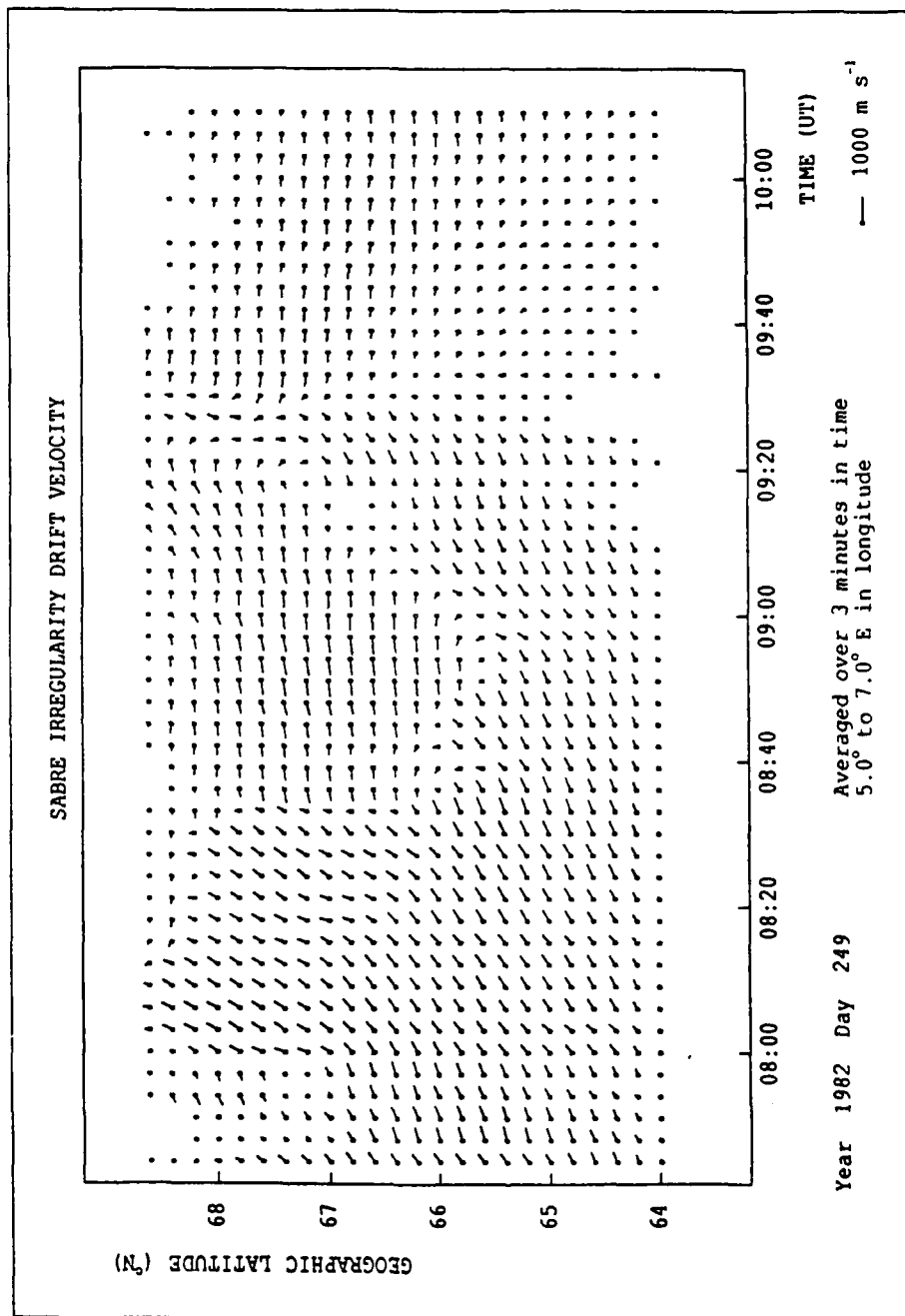


Fig. 11

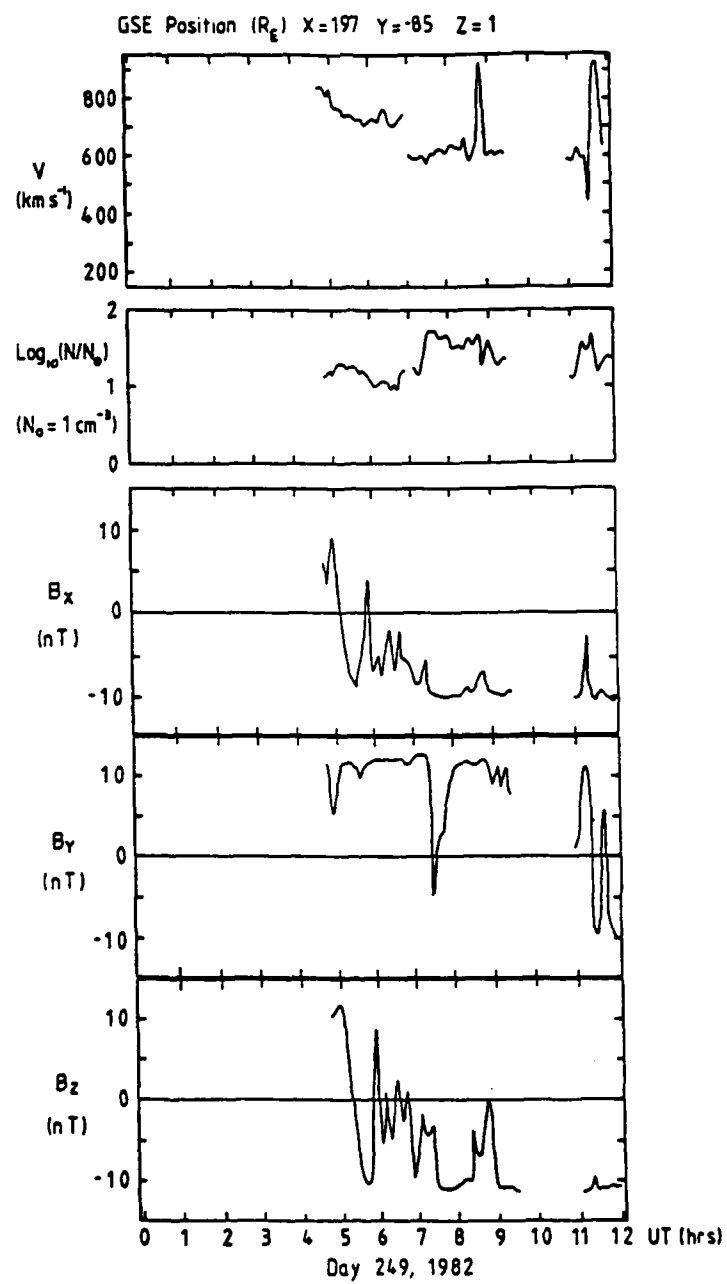


Fig. 12

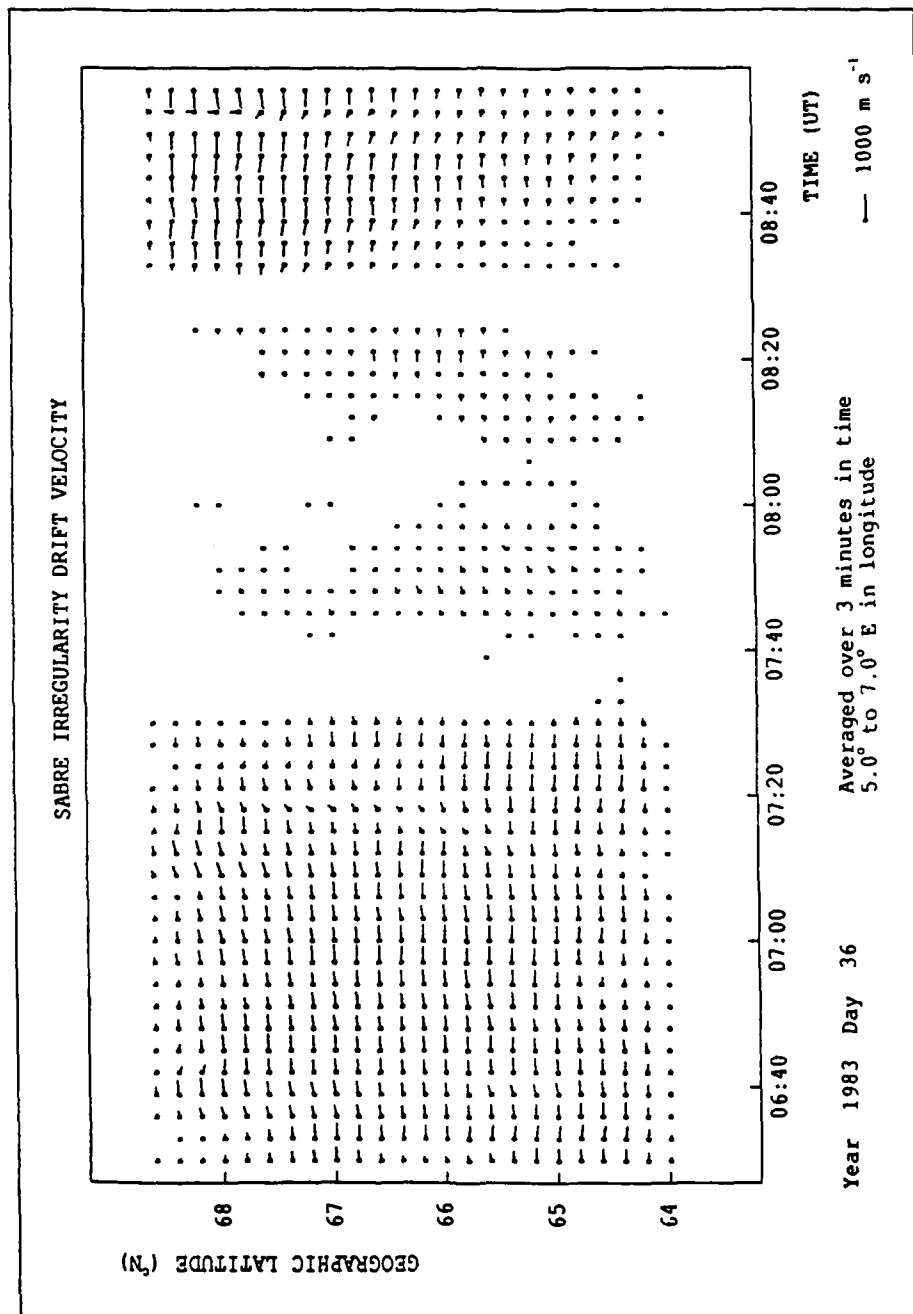


Fig. 13

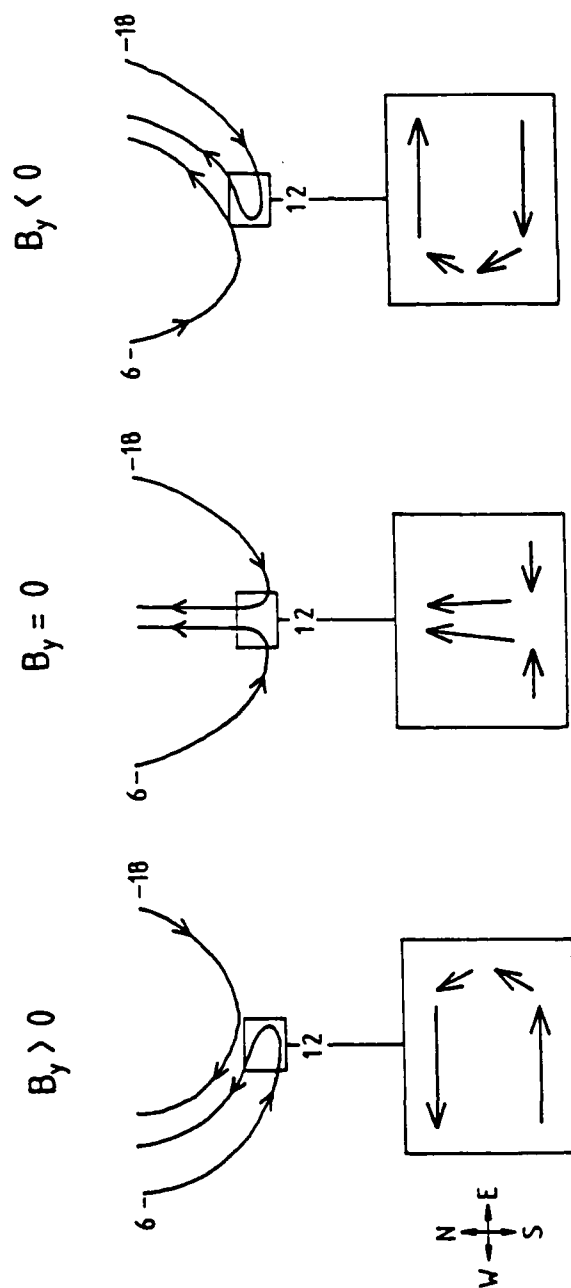


Fig. 14

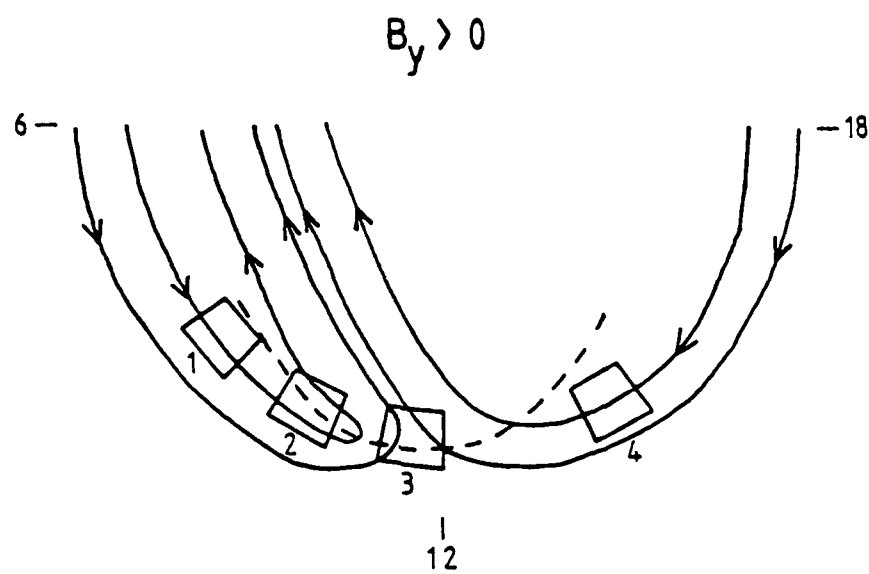


Fig. 15

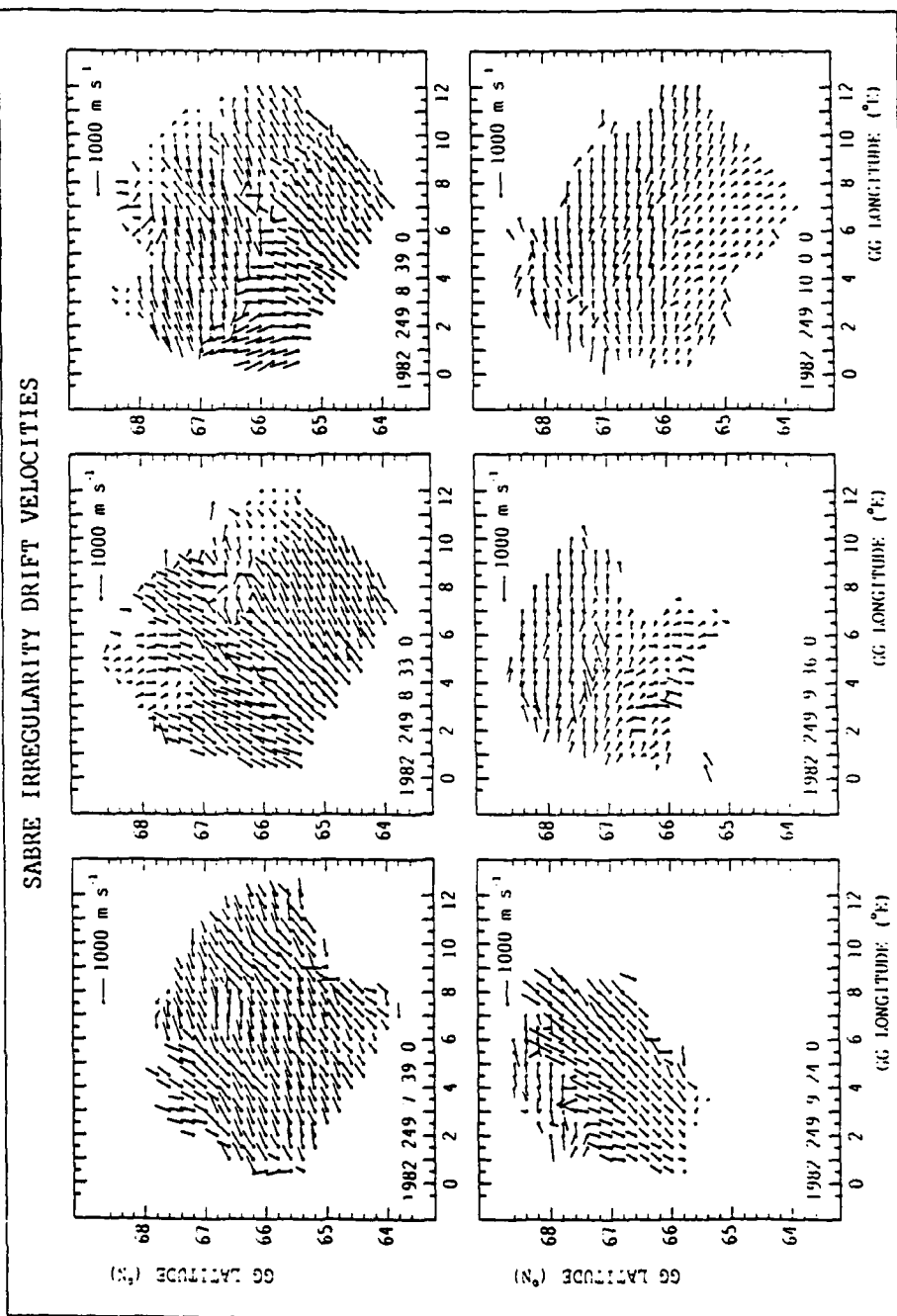
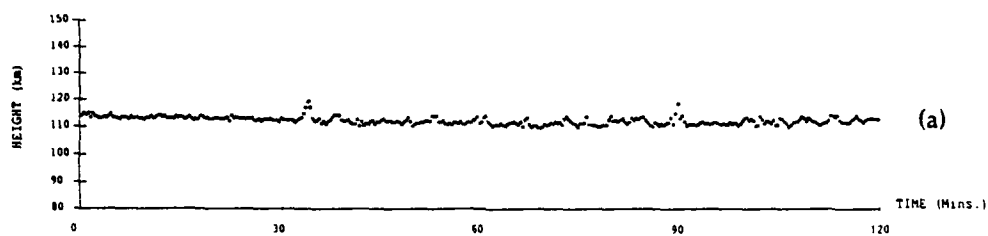
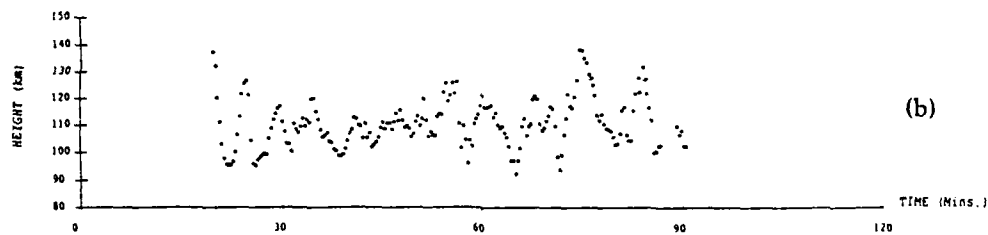


Fig. 16



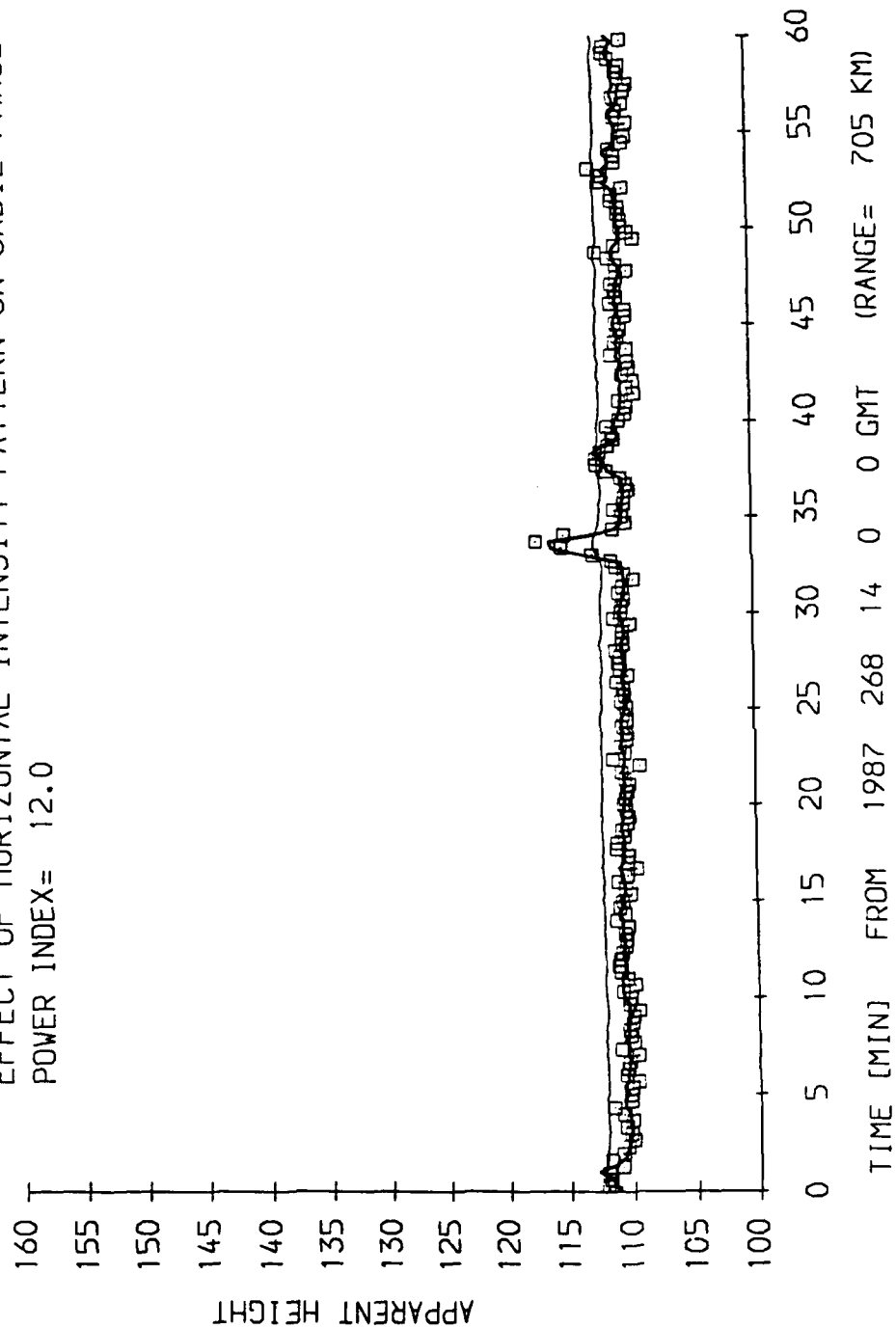
Data from 25th Sep. 1987. Starting at 14:00:00 GMT. Range is 705 km. Plot duration is 2 hours.



Data from 3rd Dec. 1987. Starting at 15:00:00 GMT. Range is 930 km. Plot duration is 2 hours.

Fig. 17

EFFECT OF HORIZONTAL INTENSITY PATTERN ON SADIE-PHASE
POWER INDEX= 12.0



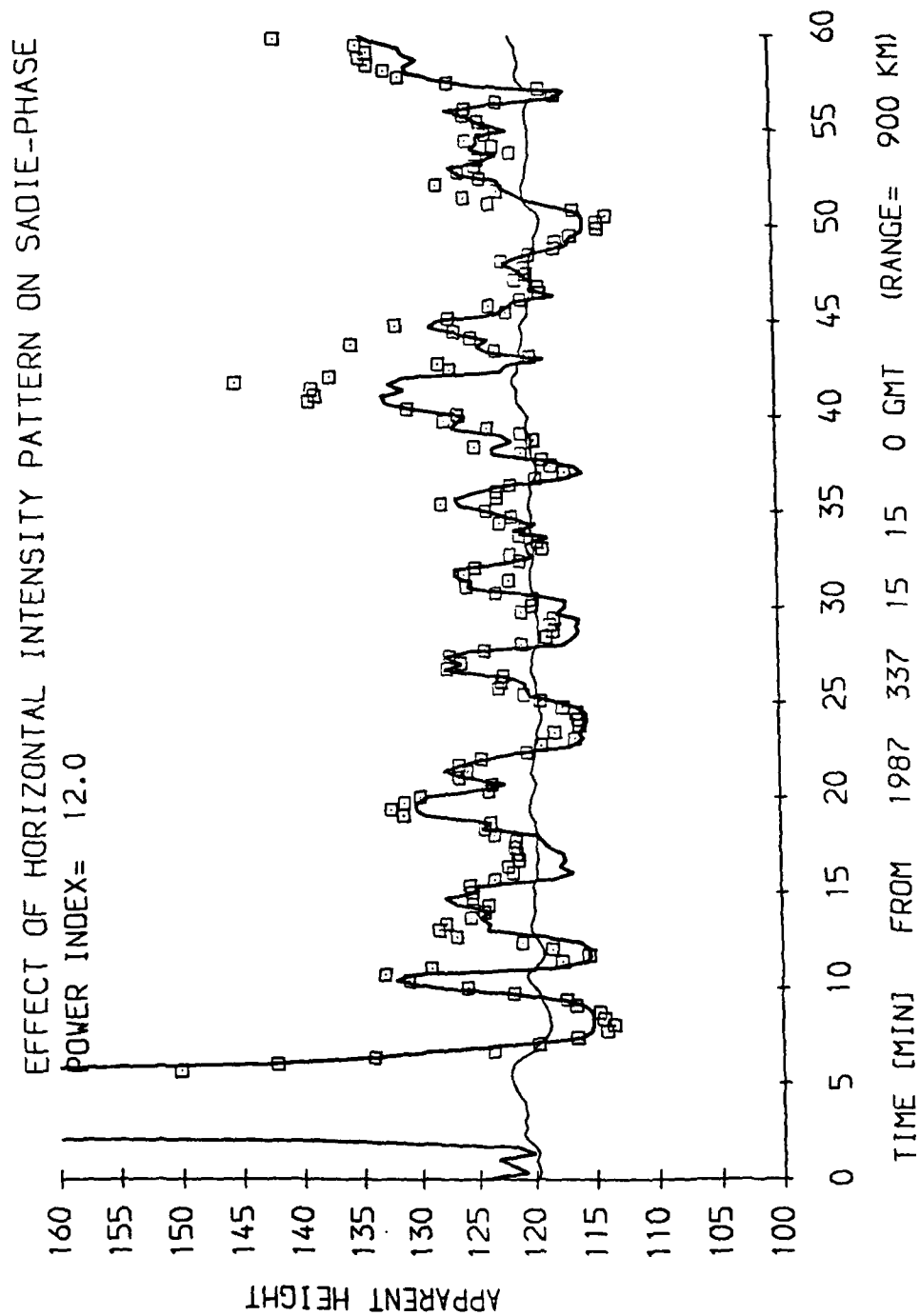


Fig. 19

SADIE AVERAGED 'HEIGHT' AGAINST RANGE

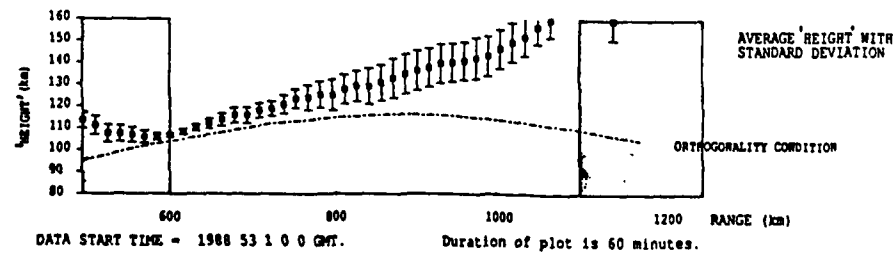
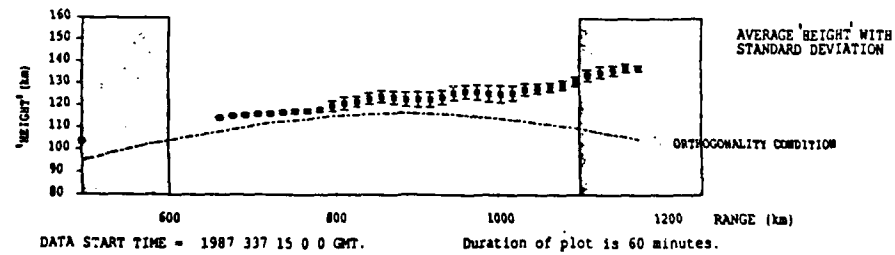
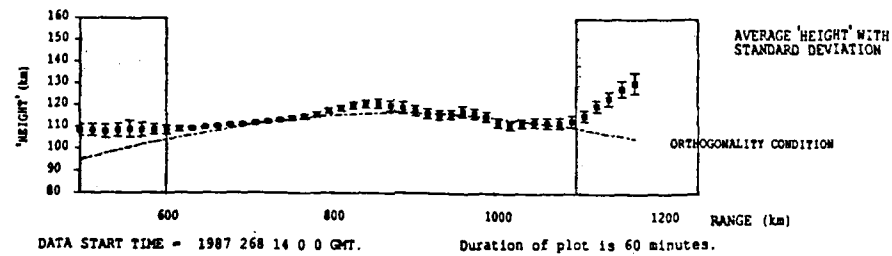
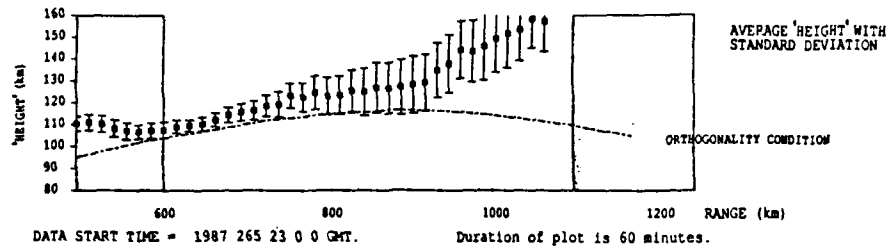


Fig. 20